DØ note #2176
July 13, 1994

Measurement of Jet Shapes from Transverse Energy Flow

Brad Abbott
Purdue University

Kathleen Streets
New York University

Abstract

The distribution of transverse energy in a jet has been measured for both the central and forward regions and at different transverse energy regions. Comparisons to Monte Carlo simulations and NLO theory are presented.

1 Introduction

Recent advances in the theoretical understanding of jet production at hadron colliders permit quantitative comparisons to experiment [1]. Next-to-Leading order (NLO) predictions at α_s^3 are possible for many hard QCD processes. These processes determine the transverse energy deposition in a jet. This study was undertaken to determine how accurately the internal structure of a jet is described by theoretical predictions.

One difficulty with jet physics is the definition of a jet. At the basic theoretical level, a jet is composed entirely of partons, i.e. quarks and gluons, and no fragmentation effects are included. This simplification works well for many QCD calculations. Calculations at this level describe many experimental processes well including inclusive jet production and production of dijets. At leading order (LO) only two final state partons are present, and the jet shape is simply a delta function at the parton's coordinates. At NLO, jet shapes becomes more complicated because there can be three final state partons. Depending on final state clustering algorithms, one or two partons may reside in a final state jet. Fragmentation of the partons causes the jets to be less easily defined. Experimentally, a jet is typically defined as a cluster of energy located within a jet cone centered on the jet axis (η_j,ϕ_j), where η is the pseudo-rapidity defined as η=-ln(tan(θ/2)), θ is the polar angle and ϕ is the standard azimuthal angle.

The DØ detector is ideal for measuring the shape of a jet due to the calorimeter's fine segmentation and high eta coverage. Other experiments have measured the transverse energy flow [2], [3] with tracking chambers, considering only the energy carried by charged particles. In the measurement described below using the DØ calorimeter, both neutral and charged particles contribute to the jet shape.

2 Data Analysis

2.1 Experimental Definition of Jets

In DØ jet energy is defined as the sum of the energy of calorimeter towers (.1 $\times$ .1 in $\eta - \phi$) which fall within the jet cone, R,

$$\sqrt{(\eta_j - \eta_t)^2 + (\phi_j - \phi_t)^2} \leq R$$

where (η_t,ϕ_t) is the center of the calorimeter tower. Each tower η is taken with respect to the interaction vertex, which is found from tracking. The jet direction is defined as

$$\eta_j = -ln(tan(\theta_j/2))$$

$$\phi_j = tan^{-1}\frac{\sum_i E_{yi}}{\sum_i E_{xi}}$$

where

$$\theta_j = tan^{-1}\frac{\sqrt{\sum_i E_{xi}^2 + \sum_i E_{yi}^2}}{\sum_i E_{zi}}$$

$$
\begin{aligned}
E_{xi} &= E_i sin(\theta_i) cos(\phi_i) \\
E_{yi} &= E_i sin(\theta_i) sin(\phi_i) \\
E_{zi} &= E_i cos(\theta_i)
\end{aligned}
$$

This is different than the definition agreed upon at Snowmass [4]. The transverse energy of a jet is defined as

$$E_{Tj} = \sum_i E_{Ti}$$

$$E_{Ti} = E_i sin(\theta)$$

where the sum over i is over all towers that are within the jet radius R. Towers above 1.0 GeV are used as seed towers for finding preclusters, which are formed by adding neighboring towers within a radius of 0.3 to seed towers. A cone of radius R is drawn around each precluster and its jet center is calculated. Using this new jet center, this process is then repeated until a stable jet center is found. An 8 GeV minimum transverse energy cut is applied to the jet finding algorithm.

After the preliminary set of jets has been found, overlapping jets can be merged or split, depending on the amount of energy contained in the overlap of two jets. Two jets are merged into one jet if 50% of the lower jet's E_T is contained in the overlap region, and the center of the new jet is defined as the vector sum of the original two jet centers. The energy of the merged jet is the sum of the energy of the original two jets. If less than 50% of the lower jet's E_T is contained in the overlap region the jets are classified as split. In this case, the jet directions stay the same and the energy of each cell in the overlap region is assigned to the nearest jet.

2.2 Experimental Measurement of Jet Shape

Jets are found using the fixed cone algorithm described earlier with radius $R = \sqrt{\Delta\eta^2 + \Delta\phi^2} = 1.0$. A large radius was used in order to minimize out-of-cone effects. To study the internal structure of jets by measuring the transverse energy flow, the jet cone is divided into 10 subcones around the jet axis with equal thickness (= 0.1 in $\eta - \phi$ space). The integrated transverse energy in a subcone is measured as a function of the radius, r, of the subcone:

$$\rho(r) = \int_0^r E_T \equiv \frac{\sum_{x=0}^{r} E_T(x)}{\sum_{x=0}^{R} E_T(x)}$$

The quantity under study is the integrated transverse energy as a function of the radius of the subcone.

The transverse energy in each subcone was obtained by looping over all cells in the jet. A cell was considered to be in a subcone if the center of the cell fell within the subcone boundary. Since some jets can be split or merged, the edges of the jets are not always smooth, however, this only affects the 10th (outermost) subcone. The sum of the E_T of all the cells within a jet should approximately equal the jet E_T, which is the sum of the E_T of all the towers, not the cells. Figure 1 shows the total cell E_T divided by the jet E_T. Non-unity in Figure 1 can be attributed to the fact that the towers are projective from a vertex at z=0, the center of the interaction region. Any vertex away from the origin permits a tower to be within a jet, but a cell within that tower to be outside the jet. As can be seen in figure 1, this is a small 1% effect.

2.3 Triggers

Four different triggers were used for this analysis: Jet_Low, Jet_Medium, Jet_High and Jet_Max. The level 1 and level 2 trigger thresholds are listed below in Table 1. Also listed in the table is the range of offline reconstruction jet E_T where each trigger is greater than 95% efficient. Both the level 2 threshold and the offline reconstruction jet E_T are for jets reconstructed with a conesize of 0.7. For the L1 thresholds column, the entry 2,7 means 2 trigger towers above 7 GeV. A trigger tower is 0.2×0.2 in $\eta - \phi$ space, larger than the standard 0.1×0.1 tower.

Table 1: Triggers Used in Jet Shape Analysis

TABLE 1

Trig Name	L1 threshold	L2 threshold GeV	Energy Range Used GeV
Jet Low	1,3	30	45-70
Jet Medium	2,7	50	70-105
Jet High	3,7	80	105-140
Jet Max	4,5	115	140-

2.4 Data Sample and Cuts

The data was taken during the 1992-1993 run of the Tevatron. Approximately 16 pb^{-1} of data was accumulated. A subset of this data was used in this analysis. Runs that were determined to be bad because of beam or hardware conditions were removed from the sample. Two types of cuts were placed on the data, cuts on each event and cuts on each jet.

For each event the trigger bits set corresponding to one or more of the four triggers in table 1 were examined. The E_T of the leading jet that was reconstructed with a conesize of 0.7 was required to be in the 95% efficiency range for one of the set bits. The condition that the missing E_T in the event was less than $0.7 \times E_T$ of the leading jet was also applied. The vertex was

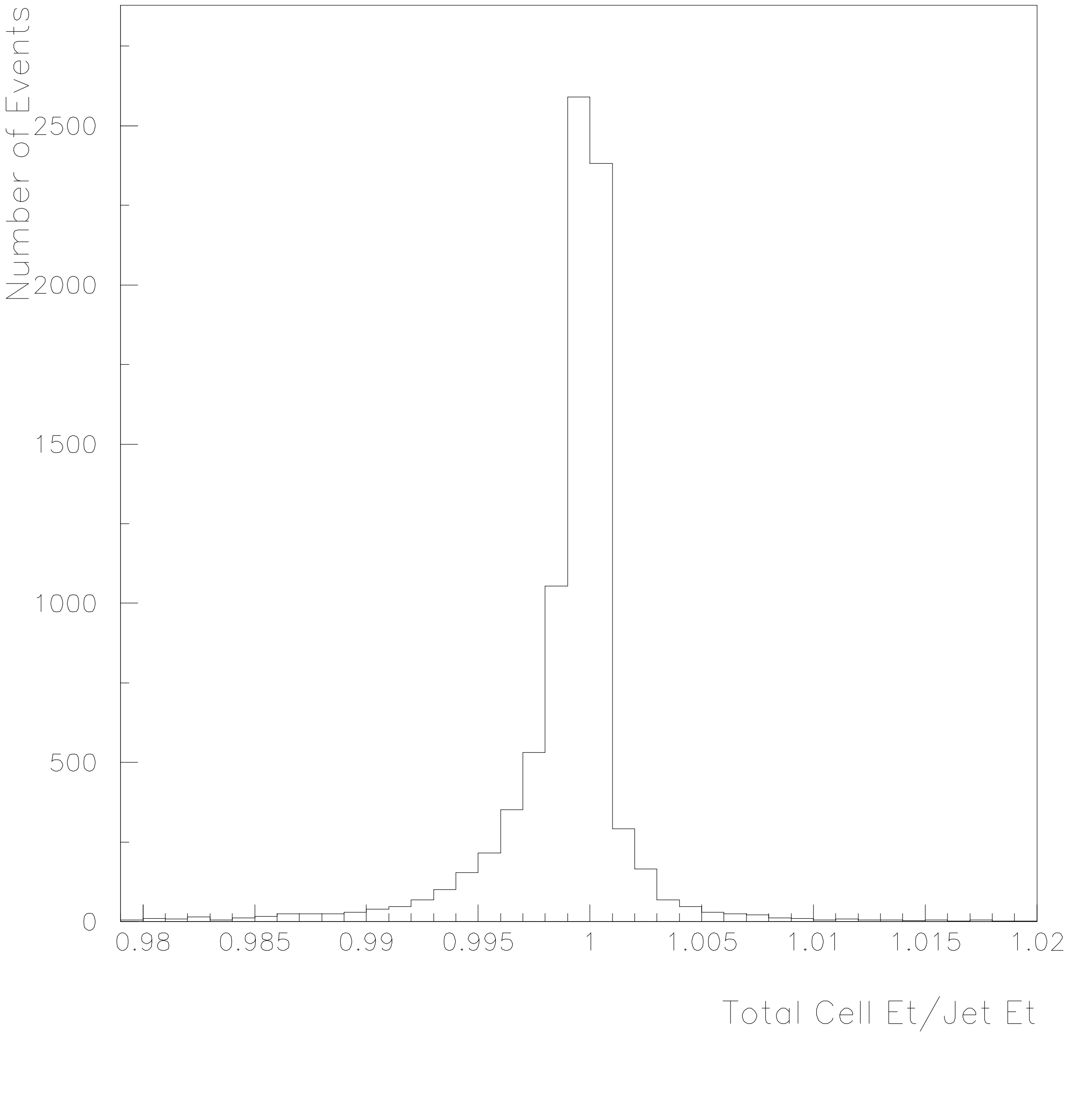

Figure 1: The ratio of the sum of the E_T of the cells in a jet divided by the jet E_T

required to be within $\pm$ 30 cm to keep the towers projective. All jets in the event were then considered if these three event cuts were satisfied.

Each jet in the event was required to pass the standard good jet cuts[5]:

- CH Fraction ≤ 0.4
- $0.05 \leq$ EM Fraction ≤ 0.95
- Cell Ratio ≤ 10

where CH Fraction is the fraction of energy contained in the coarse hadronic layers of the calorimeter, the EM Fraction is the fraction of energy contained in the electromagnetic layers of the calorimeter, and the Cell Ratio is the ratio of the most energetic cell in the jet to the second most energetic cell. These cuts were designed to remove bad jets caused by hot cells and main ring contamination.

Jets were analyzed in two different rapidity regions, a central rapidity of $|\eta| \leq 0.2$ and a forward region of $2.5 \leq |\eta| \leq 3.0$; and the four different E_T regions listed in Table 1. The restrictive η cuts were used to keep the edges of jets away from the ICD (inter-cryostat detector) region located at $\sim 1.3 \leq |\eta| \leq 1.7$.

Detector η was used for the η cut instead of physics η. Detector η is taken with respect to z=0, while physics η is taken with respect to the primary event vertex. Physics η of 0.2 with a vertex of z=30 cm corresponds to detector η of 0.5. A jet centered at 0.5 detector η would overlap the ICD region. A more restrictive 10 cm vertex cut would remove much of this overlap but reduces statistics. The jet shape was measured using physics $\eta \leq 0.2$ and a vertex cut of 10 cm. It was also measured for detector $\eta \leq 0.2$ and a vertex cut of 30 cm. The two jet shapes were virtually identical, so it was decided to used detector η for the η cut in order to increase statistics and to minimize the ICD overlap.

2.5 Corrections to the Data

The jet energy distribution must be corrected for energy from the underlying event and zero suppression and for the jet energy scale. The underlying event and zero suppression artificially increase the energy in a jet. The jet energy scale correction boosts the energy of a jet between 20% and 25%.

The jet energies were corrected by using the standard jet correction algorithm [6]. Several methods of calibration were used to obtain this jet correction. First the electromagnetic section of the calorimeter was calibrated to the Z mass peak by from using $Z \rightarrow e^+e^-$ decays. Next jets in the central region were calibrated to the electromagnetic section by using direct γ events or di-jet events in which one jet is highly electromagnetic. Then the forward regions were calibrated to the central region by comparing di-jet events in which one jet is central and the other forward. This comparison was done using jets with a cone radius of 0.7. However, the method is fairly insensitive to cone size with only a 1-2% difference expected between a cone size of 0.7 and a cone size of 1.0. The jet correction algorithm also subtracts the effects of uranium noise and underlying event correctly for a 1.0 cone. In this data analysis, the corrected jet energy was used only for binning and no attempt was made to apply the jet energy scale correction individually on each subcone.

The magnitude of the underlying event and zero suppression effects were measured from a minimum bias run. The underlying event was constant in E_T at 0.55$\pm$ 0.1 GeV/$\eta \cdot \phi$. The zero suppression increase was constant in energy at 1.36$\pm$ 0.2 GeV/$\eta \cdot \phi$. Both of these effects were subtracted from each individual subcone. Since the underlying event is constant in E_T, the amount of transverse energy in each subcone is simply the product:(0.55 $\times$ subcone area). If a multiple interaction occured, the correction was doubled. The zero suppression is constant in energy, so an integration is required in order to determine the amount of transverse energy in a subcone:

$$\text{zero supp. correction(GeV)} = \int\int 1.36 \sin\theta \, d\eta \, d\phi$$

The magnitude of uranium noise was calculated for each jet and was removed for each subcone.

Zero suppression effects are due to the asymmetric nature of the uranium noise in the calorimeter and the 2σ cut imposed on each calorimeter cell. The uranium noise distribution has a mean of zero, but after the 2σ cut the mean is positive, since the distribution is asymmetric. If every cell in a jet cone has energy due to the hard scatter there would be no effect from uranium noise, since the energy would be far above pedestal and the 2σ cut. The affect of zero suppression depends directly on the percentage of cells in a jet outside the 2σ cut. The percentage of cells with energy during a minbias run was measured to be approximately 4% in the central region and 7% in the forward region. The percentage of cells with energy in a jet with a conesize of 1.0 is approximately 10% in the central region and approximately 15% in the forward region. The difference between the data and the minbias is between 6-8%, so using the full zero suppression from minbias introduces a 6-8% error on the correction. This is within the error on the zero suppression value of 15%. The percentage of cells with energy was also measured as a function of subcone. In the center of a jet, the percentage of cells with energy can be higher than 80%, so using the zero suppression value from minbias introduces an error larger than 15%. Therefore, the zero suppression value was corrected for the percentage of cells with energy in each subcone.

The energy deposition during a minimum bias run was fit to a function that assumed a constant E_T and a constant energy. However, the magnitude of the zero suppression effect should depend on the size of the calorimeter cells, leading to a non-constant zero suppression correction. To verify the validity that both the underlying event and zero suppression values can be treated as constants, the amount of transverse energy in each subcone due to these two effects was calculated by a second method which did not assume the underlying event and zero suppression were constant. Instead of parameterizing the minimum bias data, the measured transverse energy in the calorimeter during a minimum bias run was subtracted out of each subcone. It was found that the two methods agreed very well, with the difference in any one subcone not being larger than 100 MeV for both the forward and central regions. Therefore, the assumption that the underlying event and zero suppression are constants is appropriate.

The four different triggers used in this analysis each had different prescales. Jets within each E_T interval could come from the different trigger bits. The theoretical jet shape takes into account the jet cross section by weighting each event by the jet cross section. In data in order to account for the jet cross section, each event must be weighted by the product of the trigger prescale and offline cut efficiency. The prescale values for each trigger were found by dividing the total luminosity for the runs used in this analysis by the luminosity for each trigger bit. Three of the triggers had a z-vertex while the fourth did not. An offline vertex cut was applied, so the efficiency for the vertex cut was calculated for each trigger. The trigger prescale, was determined by using the highest trigger bit that was efficient.

2.6 Systematic Errors

The systematic errors from underlying event, zero suppression and the jet energy scale on the jet shape were found by varying each correction within errors. The three errors were added in quadrature to the statistical errors to get the final total error on the jet shape. The largest error is $\sim 2\%$, due to the uncertainty in the jet energy scale. This error is related to binning, allowing jets that were in previous bins to populate the region of interest. The errors due to the uncertainty in the underlying event and zero suppression are small, on the order of 0.5%.

The standard jet quality cuts are between 97% and 95% efficient at keeping good jets [5]. The $\sim 5\%$ of the jets which are removed by these cuts are primarily narrow jets and removing them may bias the jet shape. However, the jets removed by these cuts must differ significantly from the average jet in order to affect the jet shape by more than 1%. The jet shape was measured with Monte Carlo with and without the standard jet quality cuts. It was found that the quality cuts change the jet shape by less than 1%, so a conservative error of 1% was assigned for using the jet quality cuts.

3 Results

Figure 2 shows the jet shape for four different E_T regions. The narrowing of jets with E_T is significant. All of the jets which passed the quality cuts were used in the jet shape analysis. A jet was used regardless of whether the jet was merged or split. Figure 3 shows how the jet shape changes for different merge/split criteria. The merged jets are much wider than the non-merged jets. The energy flow for all jets is very close to the energy flow for non-merged jets because few jets are merged or split.

The jet shape was also measured for the leading jet and all other jets seperately. Figure 4 shows the leading jet to be slightly narrower than the other jets.

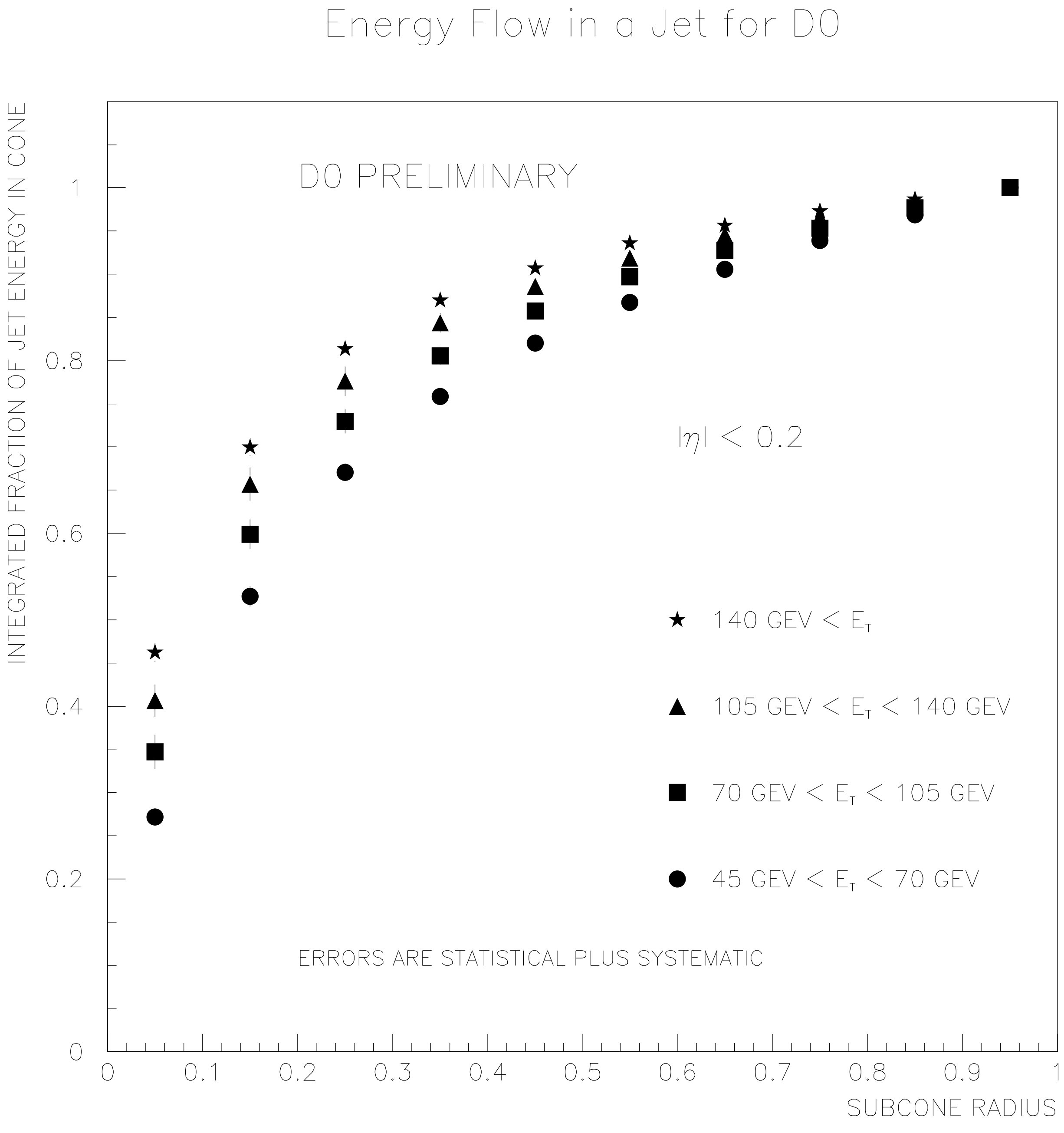

Figure 2: The jet shape in the central region for different E_T intervals

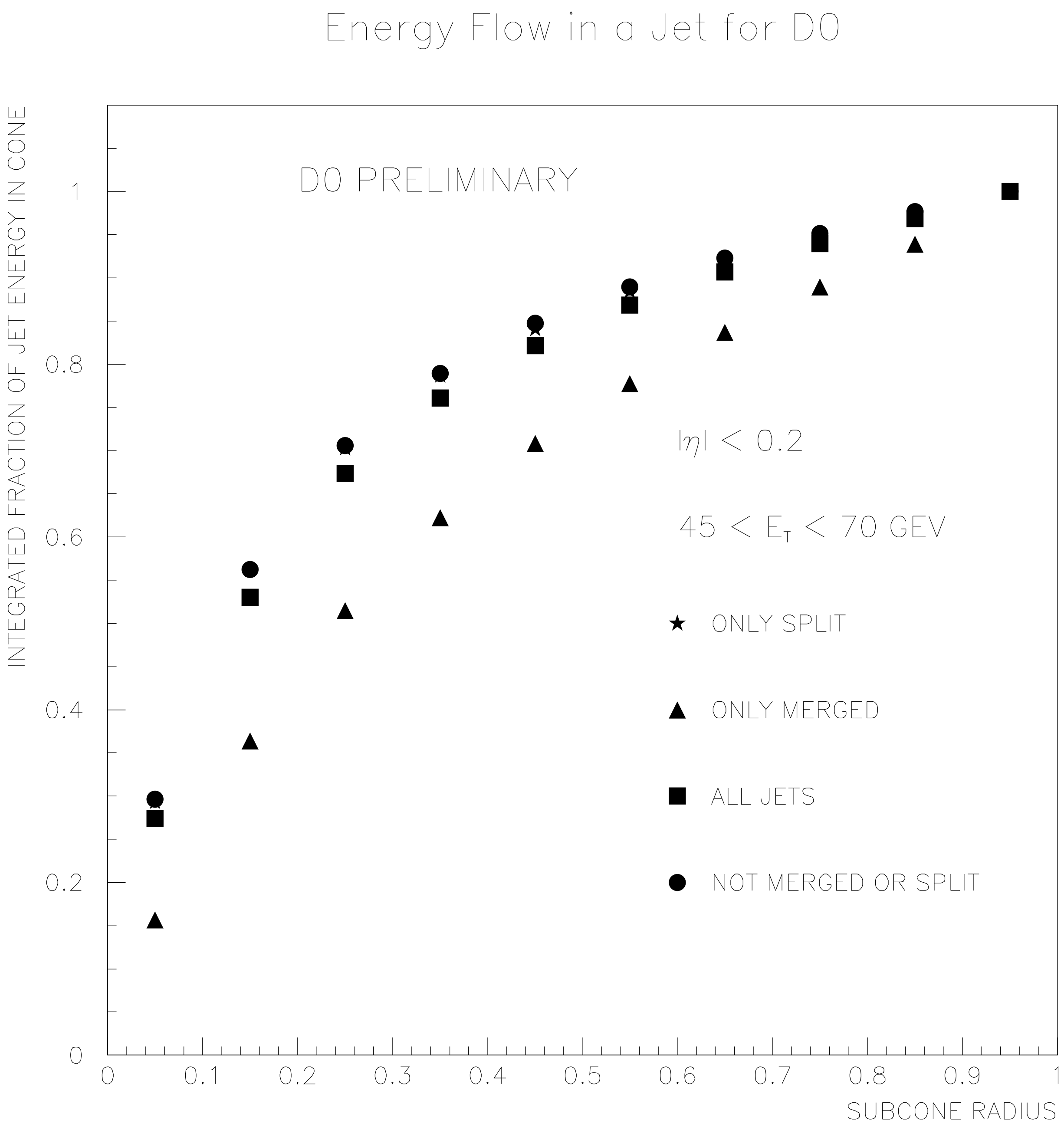

Figure 3: The jet shape in the central region for different merge/split criteria

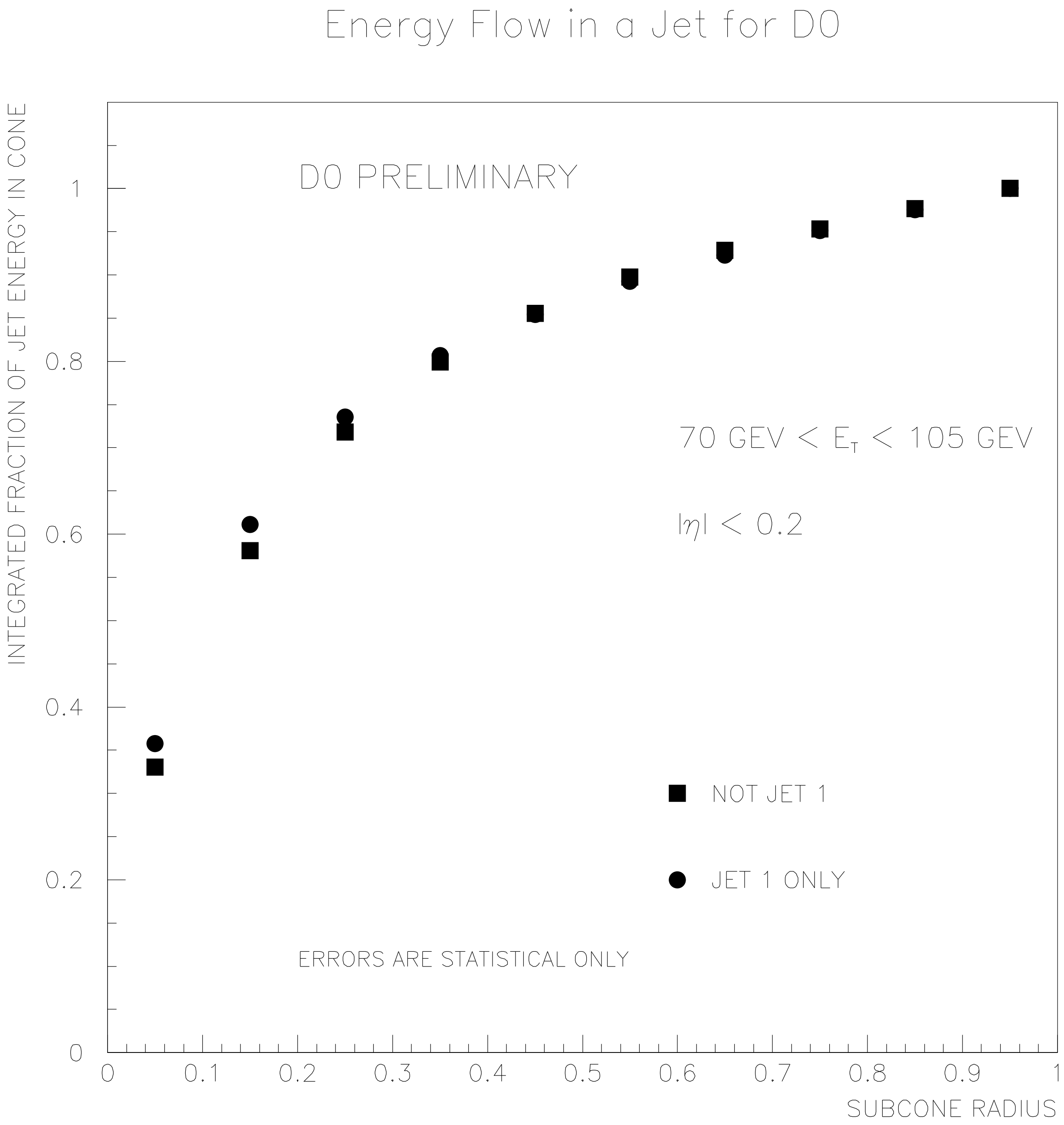

Figure 4: The jet shape in the central region for leading jets and non-leading jets.

This analysis was also performed on different Monte Carlo simulations. All of the same cuts and corrections were applied to the simulations except for the effects of zero suppression since there is no uranium noise in the Monte Carlo. In order to take into account the falling cross section of jets, each jet's shape was weighted by cross section.

Figures 5-8 compare collider data to the Monte Carlos in the central region. At the lower energies, Isajet describes the jet shape better. As the energy increases Herwig does a better job.

Figures 9 and 10 compare collider data to the Monte Carlos in the forward region. None of the Monte Carlos describe the data well. For both Herwig and Isajet the forward jets are narrower than data.

4 Effects of the Calorimeter

The effects of the calorimeter must be removed before comparing to partonic theory. The calorimeter affects the jet shape in two ways: a non-linear response narrows the jet shape and showering widens the jet shape. Non-linear response narrows the jets because the energies of particles decrease as they move further from the center of a jet, see figure 11. As the energy of particles decreases, the response moves further away from non-linearity so less energy is measured at the edge of a jet, thereby narrowing it. Showering widens the jet because the energy of a particle that strikes the calorimeter in a particular subcone may shower over many subcones.

Forward jets are reconstructed with a small η bias which tends to locate jets more centrally. This η bias is purely a calorimeter effect, mostly due to out-of-cone showering. It has been measured to be approximately 0.03 for a conesize of 0.7 in the forward region. In the central region the η bias is negligible. For the larger radius of 1.0, with reduced out-of-cone effects, the η bias will be reduced. Even if some η bias is still present in the data it is irrelevant because both the data and Monte Carlos will be biased equally so they can be directly compared. The η bias is removed when comparing to theoretical predictions because the effects of the calorimeter have been removed from the data.

To determine the effects of the calorimeter on the jet shape, three different Monte Carlo simulations were used. The jet shape was measured using Isajet, Pythia and Herwig. Three different Monte Carlo simulators were used because the effects of the calorimeter on the jet shape depend on the fragmentation of the jet. The jet shape was determined before calorimeter effects by measuring the energy flow using only the fragmented particles. The jet shape after calorimeter showering was found by using a detector simulator and measuring the energy flow using the calorimeter cells. The difference between the two measurements gives the effects of the calorimeter. Correction factors were found for each simulator which remove the calorimeter effects. Each simulator gave slightly different correction factors, so the average of the correction factors was used to assign the final overall corrections. The jet shape as measured using calorimeter cells is labeled as "Calorimeter" and the jet shape after the calorimeter effects have been removed is labeled as

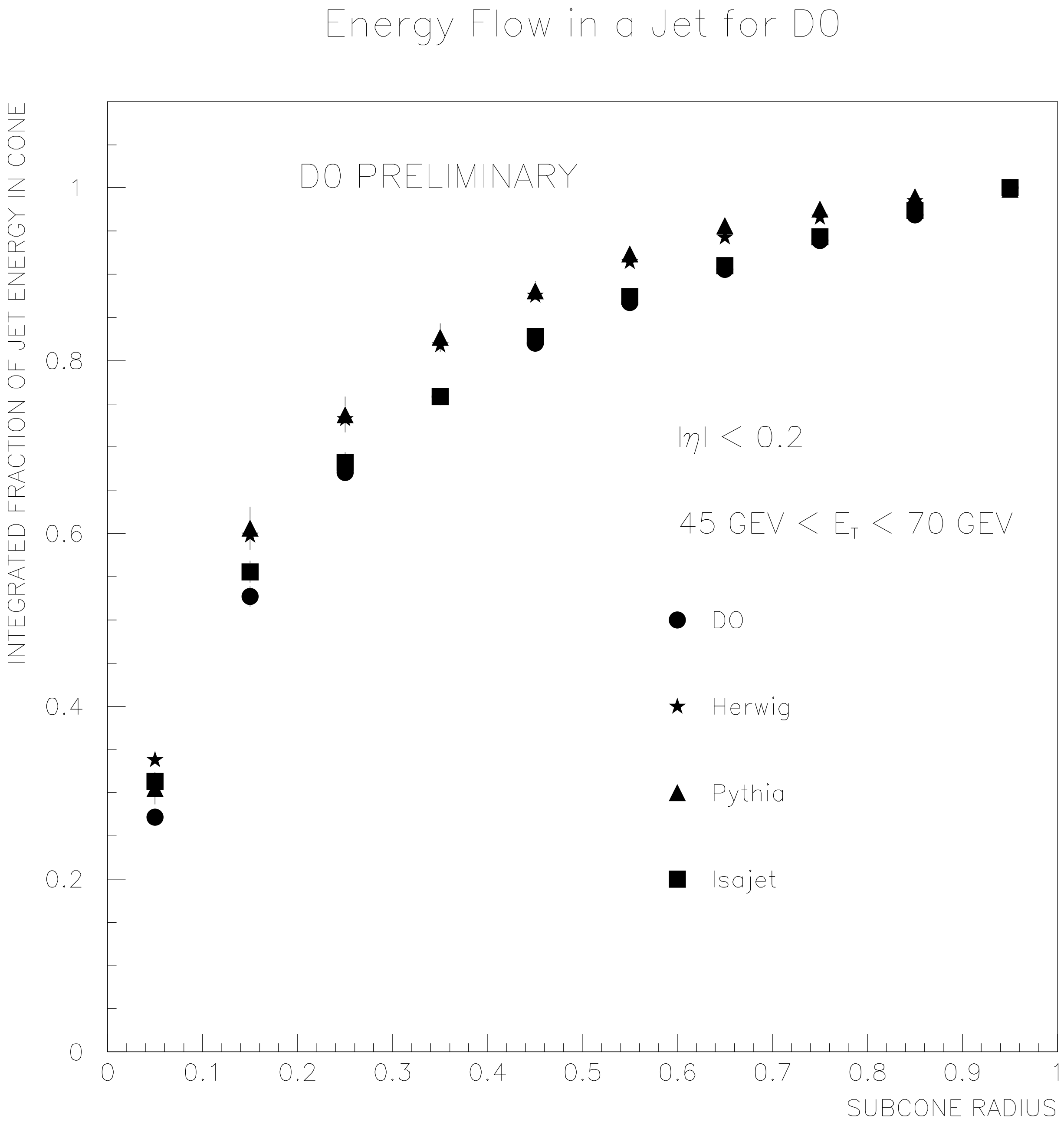

Figure 5: Comparing data to MC in the central region for 45-70 GeV jets.

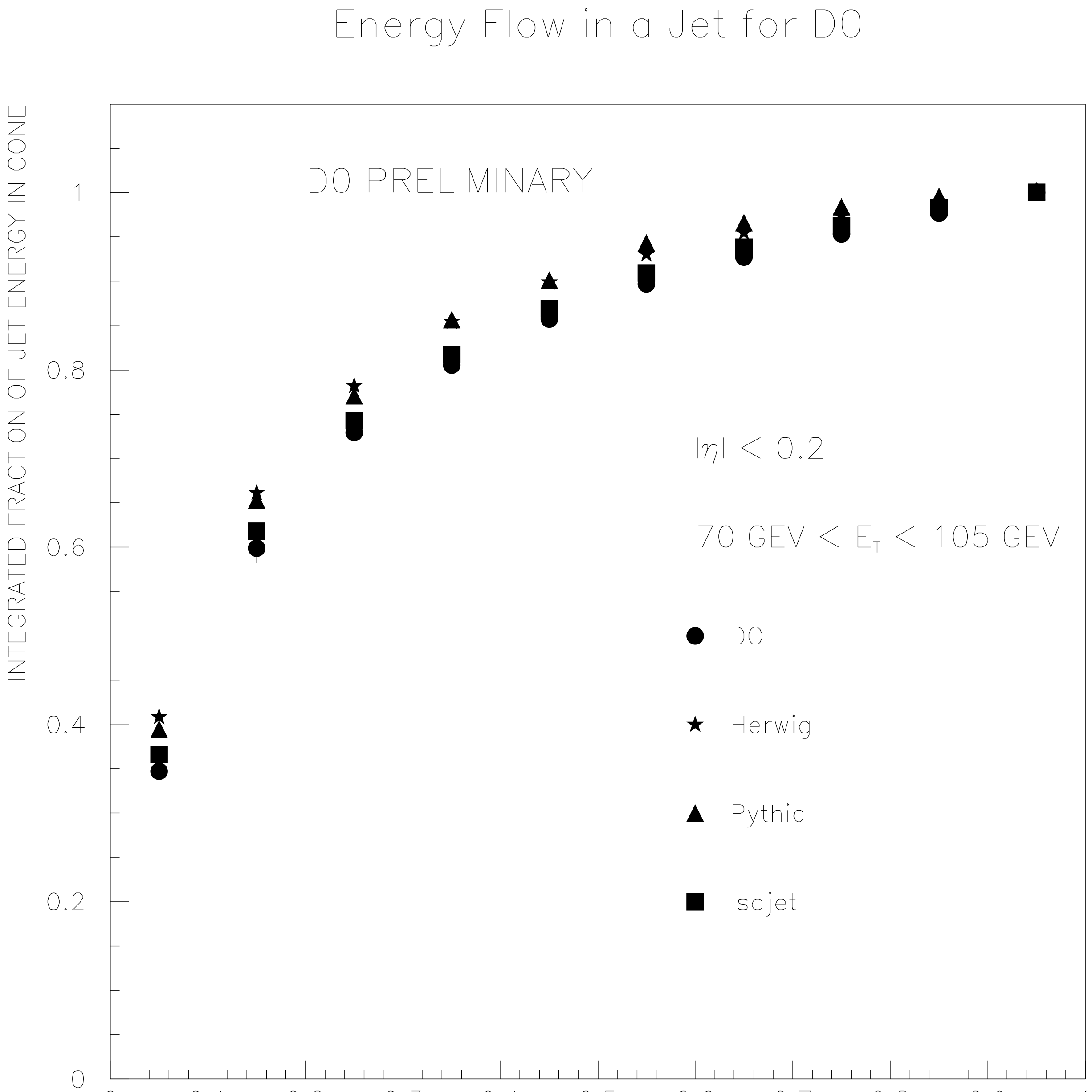

Figure 6: Comparing data to MC in the central region for 70-105 GeV jets.

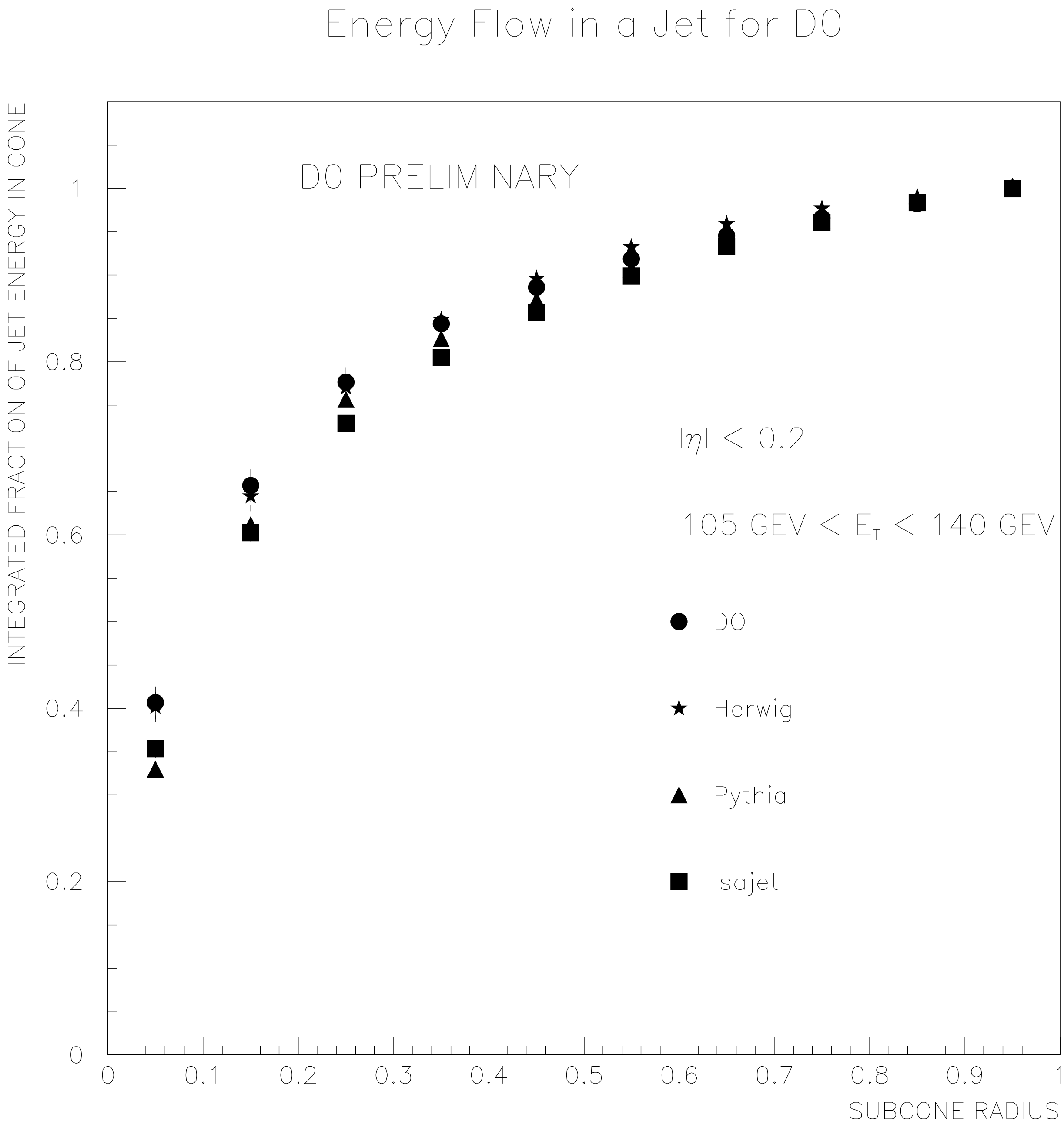

Figure 7: Comparing data to MC in the central region for 105-140 GeV jets.

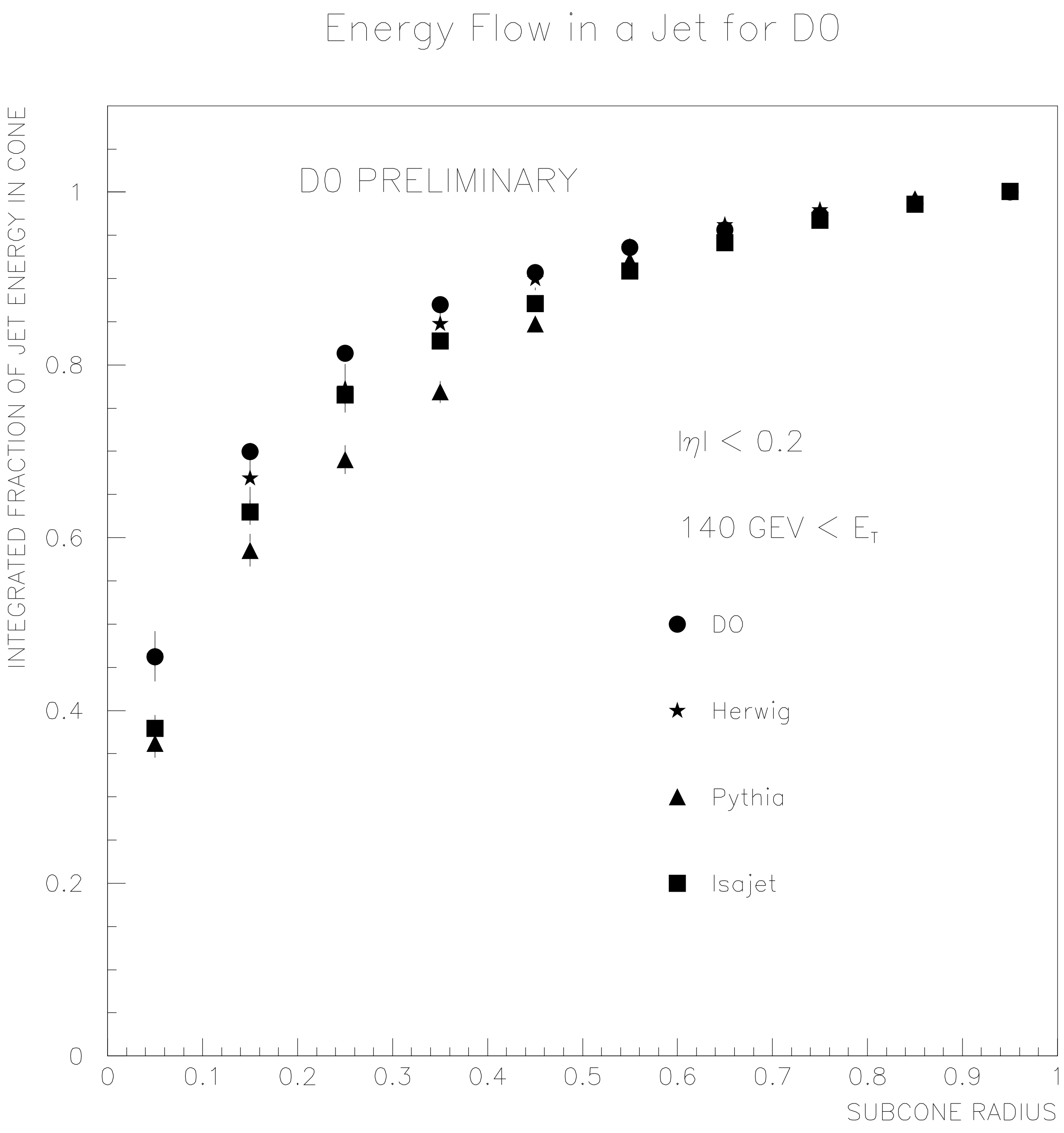

Figure 8: Comparing data to MC in the central region for 140- GeV jets.

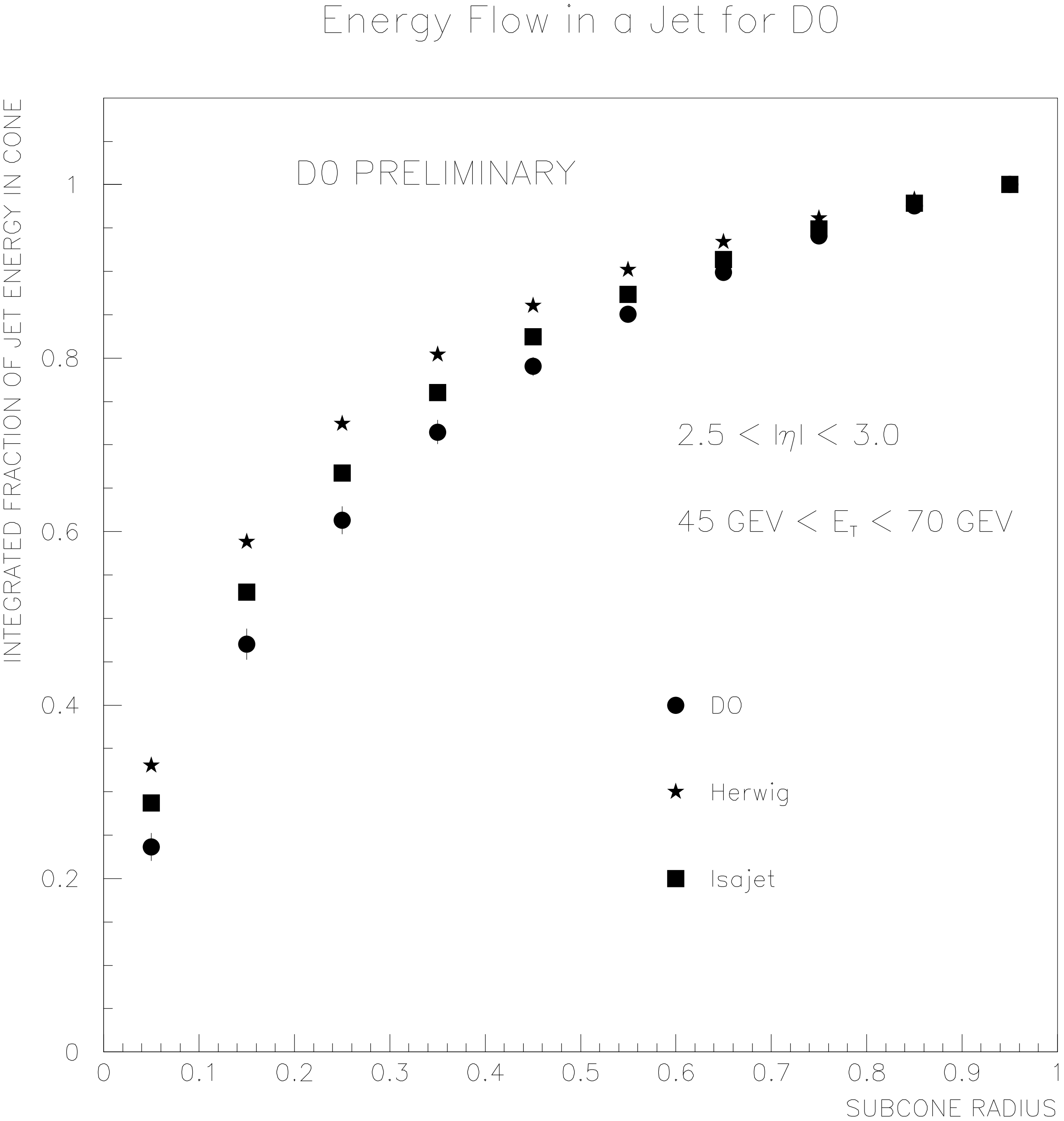

Figure 9: Comparing data to MC in the forward region for 45-70 GeV jets.

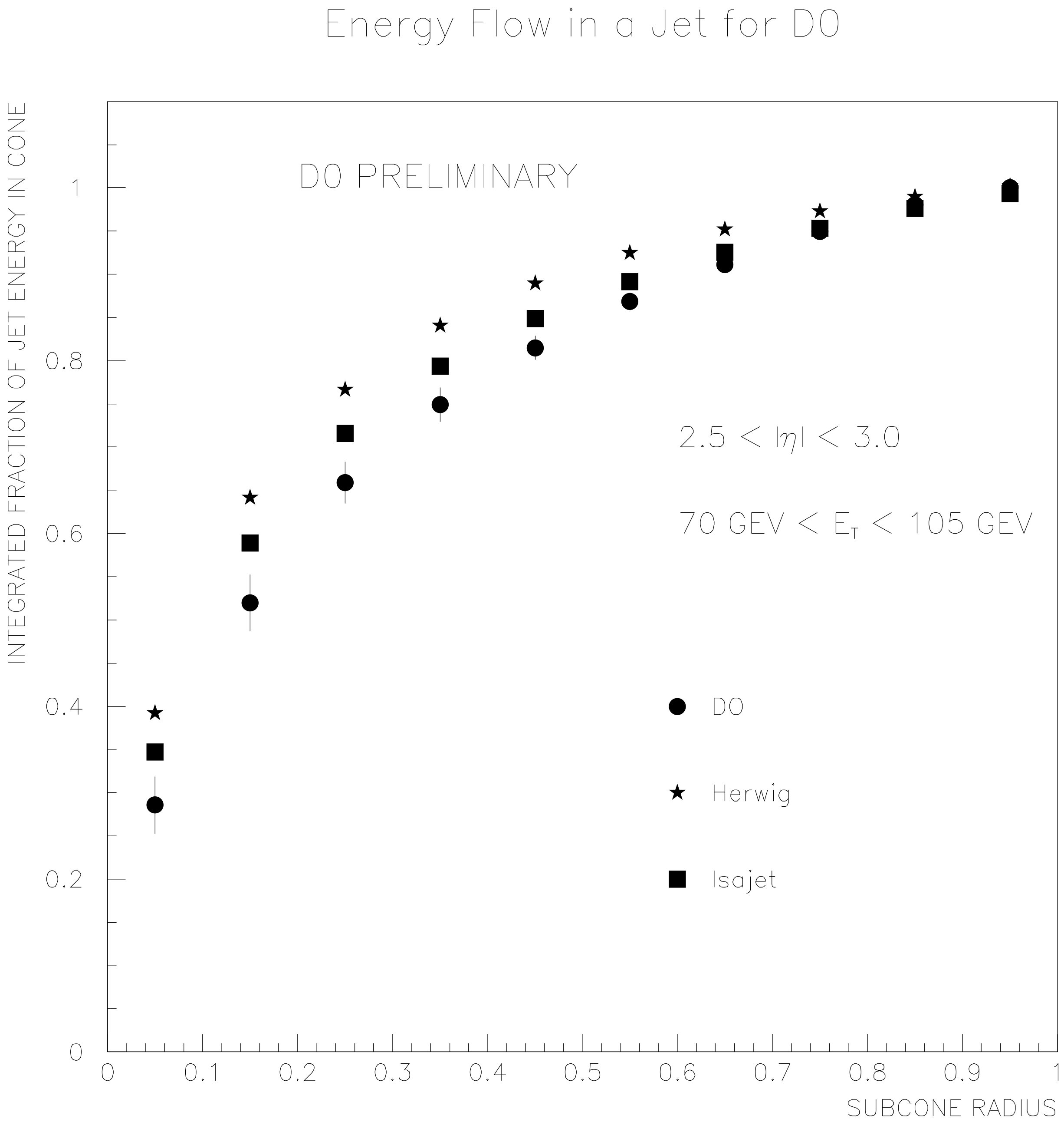

Figure 10: Comparing data to MC in the forward region for 70-105 GeV jets.

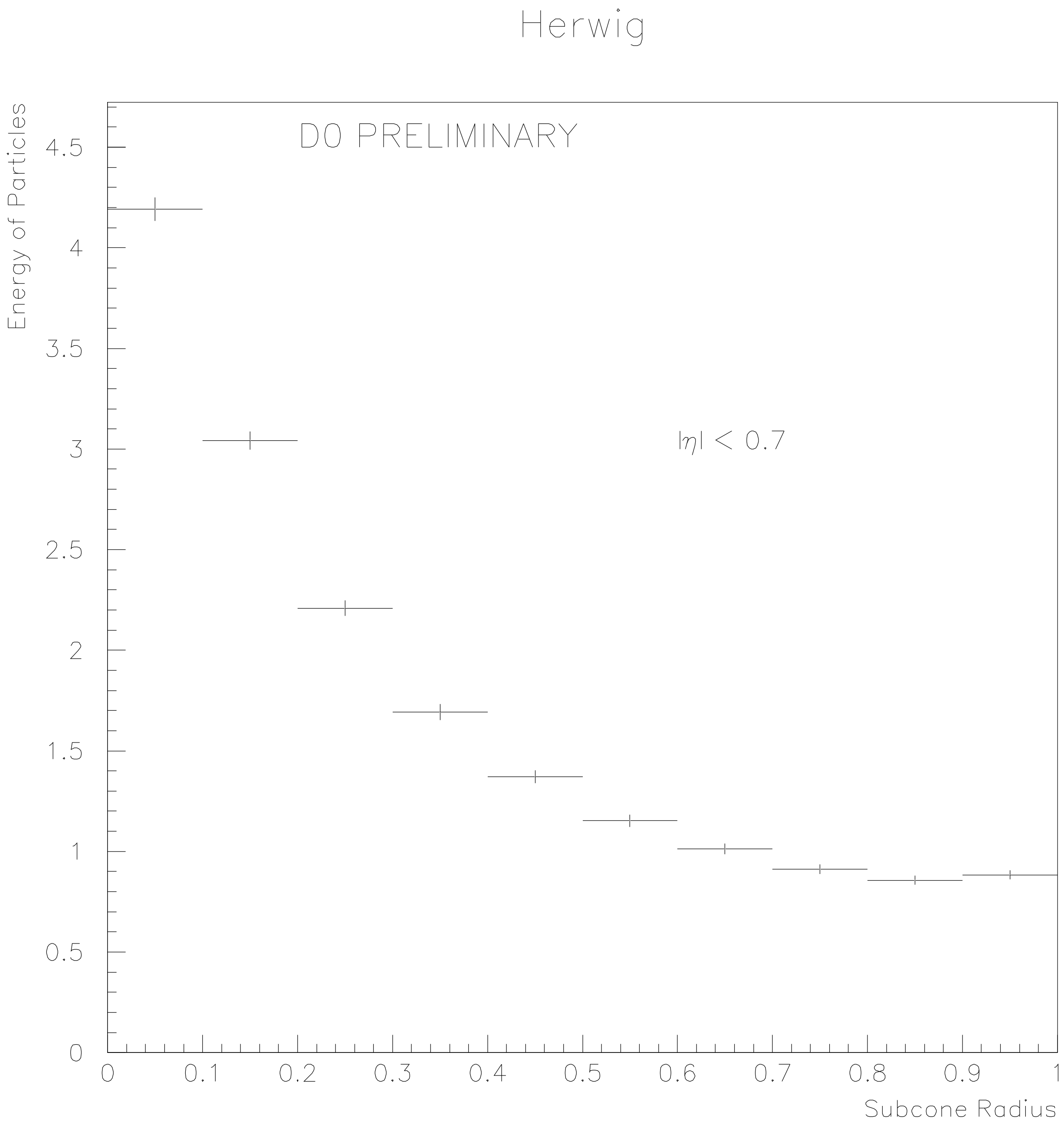

Figure 11: The average energy of particles within each subcone vs distance away from jet center.

"Particle".

Showering effects should be more pronounced in the forward region than in the central region. The shower size in $\theta - \phi$ space of a particle with energy E is the same in the central and forward regions. The physical area in $\eta - \phi$ space is smaller in the forward region so forward jets should shower over more calorimeter cells than central jets.

Figure 12 shows the differences between jet shapes before and after simulation in the calorimeter. For central jets the difference is small, but for forward jets it is quite significant.

The correction factors depend on the accuracy of the detector simulator, GEANT. To check the internal consistency of GEANT, two different geometries were used. The full plate level geometry takes into account all the known amount of material in the calorimeter. The mixture level geometry is the standard geometry and assigns an average amount of material for different $\eta - \phi$ slices. Figure 13 shows the correction factors obtained for the central region for both geometries. Both geometries give similar results. The correction factors used were additive instead of multiplicative in order to remove any normalization differences in the Monte Carlos.

Removing the effects of the calorimeter introduces another systematic error corresponding to the different simulations. This error was assigned to accomodate the extreme values among the different Monte Carlos used to find the correction factors. The error was added in quadrature to the other systematic errors described previously.

Figure 14 compares the energy flow for DØ after the effects of the calorimeter have been removed to the published energy flow for CDF. The effects of the calorimeter must be removed when comparing to CDF since CDF uses tracking chambers to determine the jet shape. Note the average energy of the jets in figure 14 is higher for DØ than for CDF and the η regions are different. The two curves agree within errors, with DØ being slightly narrower. This is consistent with DØ using higher energy jets.

Figures 15 and 16 compare central jets to forward jets. This is the first measurement of jet shape at such high η. For both E_T regions the forward jets are narrower than the central jets.

5 Comparison to Theoretical Predictions

The data can be compared to JETRAD [7], a computer generated exact NLO tree and loop level theoretical prediction. The theoretical jet shape was determined for three different renormalization scales, $\mu = 2E_T$, E_T, and $E_T/2$, where E_T refers to the average E_T of the jets in the event. The definition of E_T is not unique and different choices are possible. Another possible choice for the renormalization scale is the E_T of the leading jet in the event. There was no difference in the jet shape between the two definitions, so the definition of E_T = average jet E_T was chosen. There are many different structure functions currently available and the CTEQ2M structure function was chosen for determining the theoretical jet shape for all energies and eta regions. The MRSD- and ?? structure functions were also used to see the

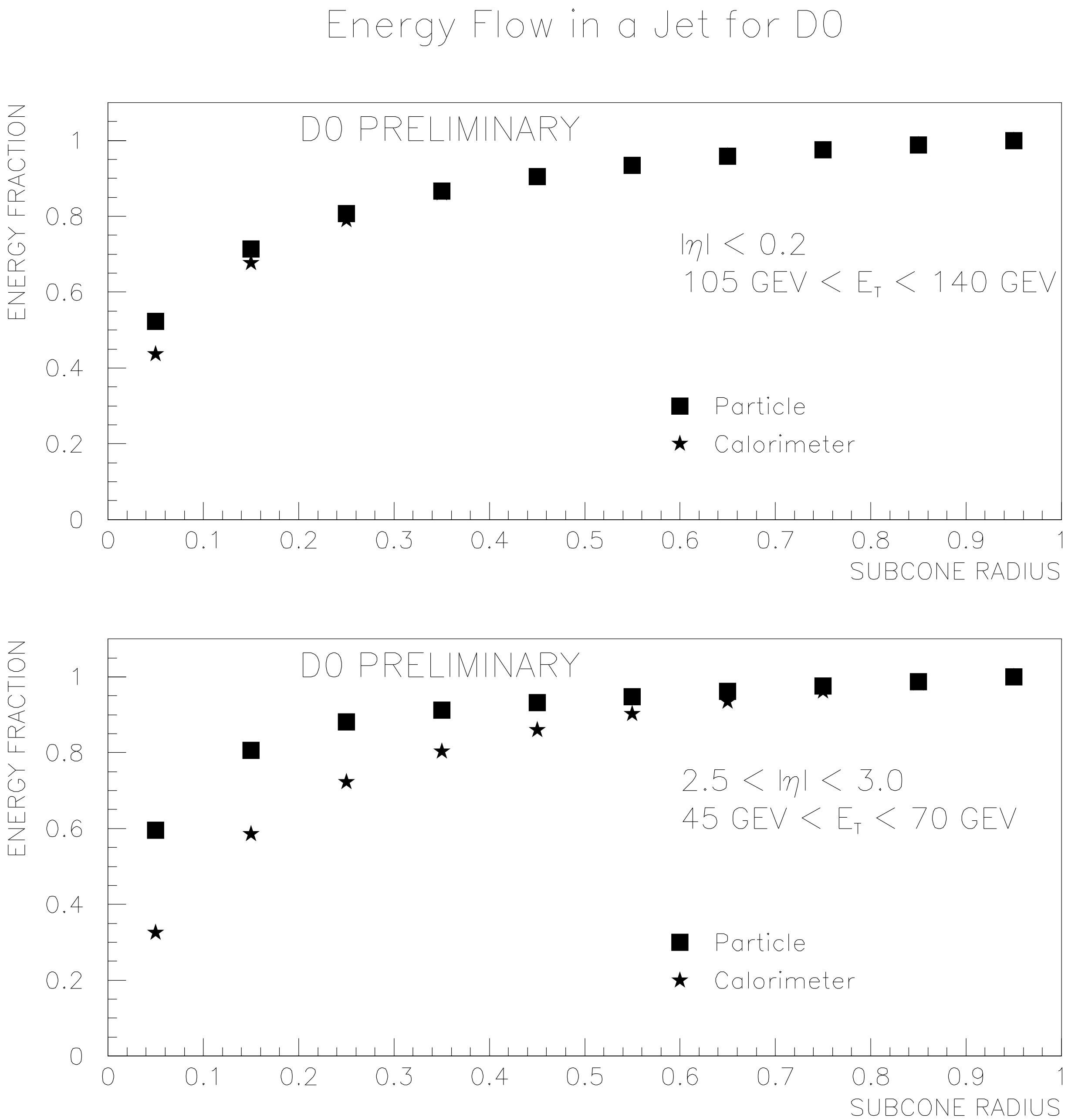

Figure 12: The difference between jet shapes before and after the calorimeter for central and forward jets.

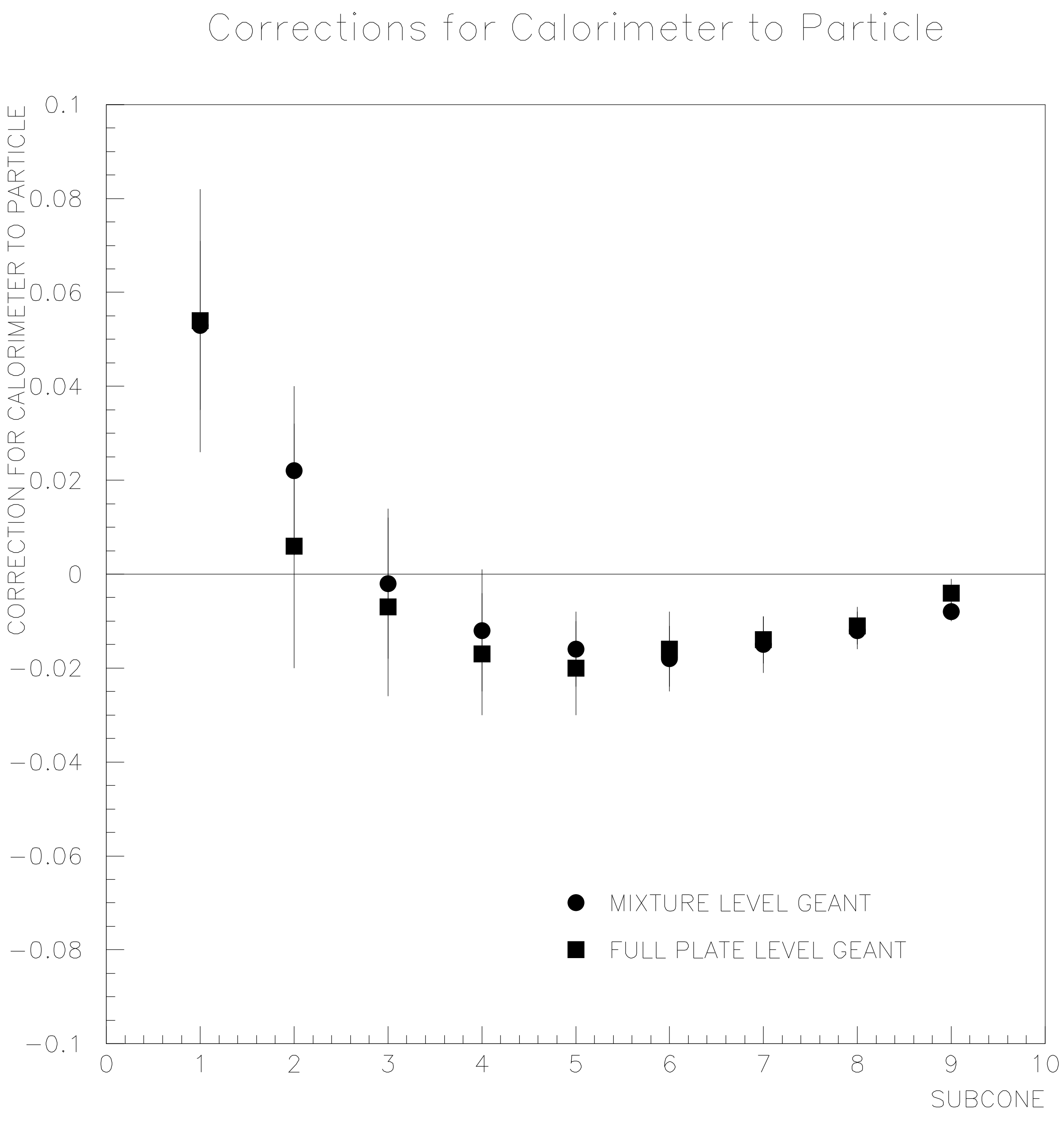

Figure 13: Correction factors for two different geometries in Geant.

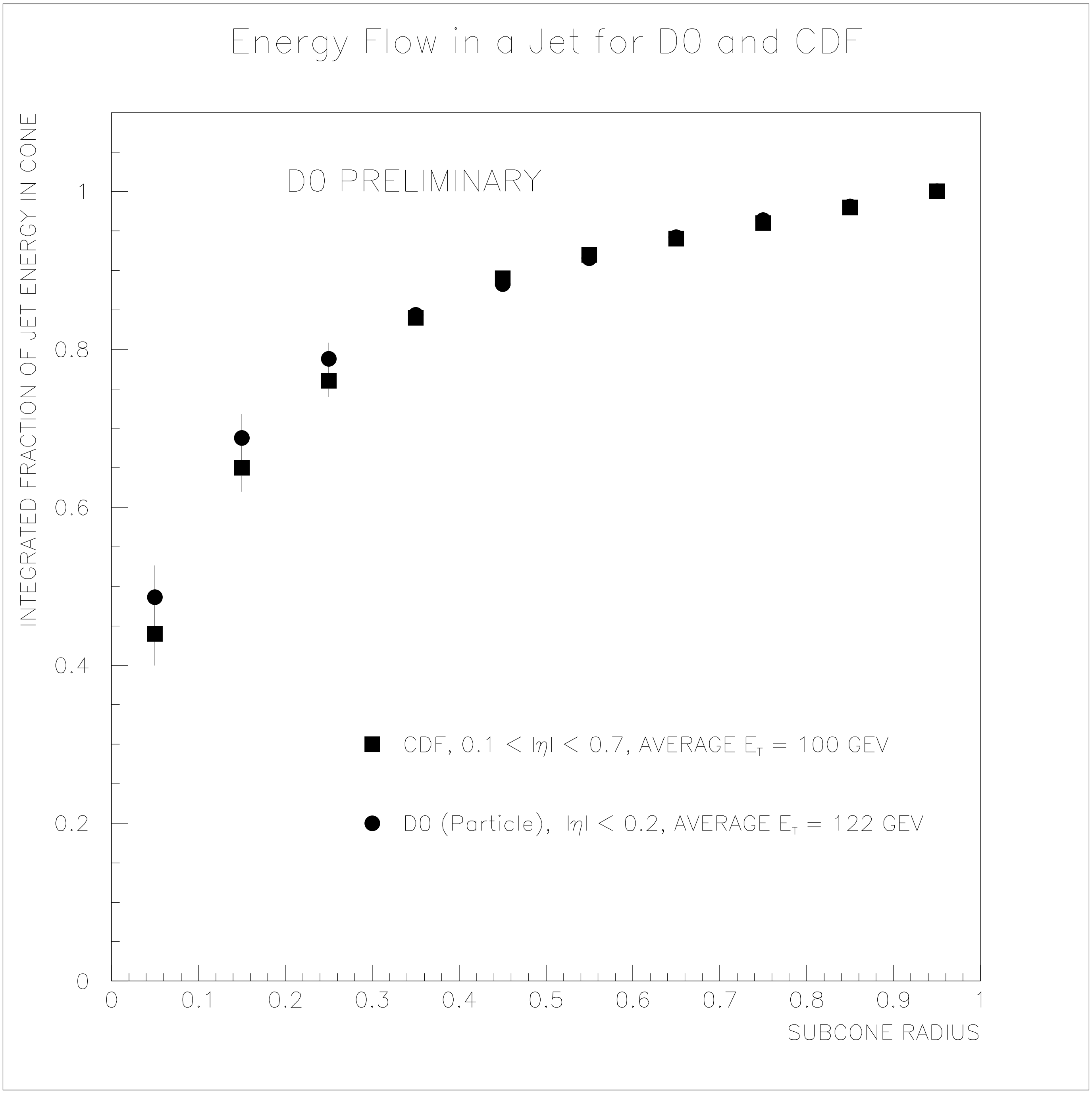

Figure 14: The jet shape at DØ and CDF.

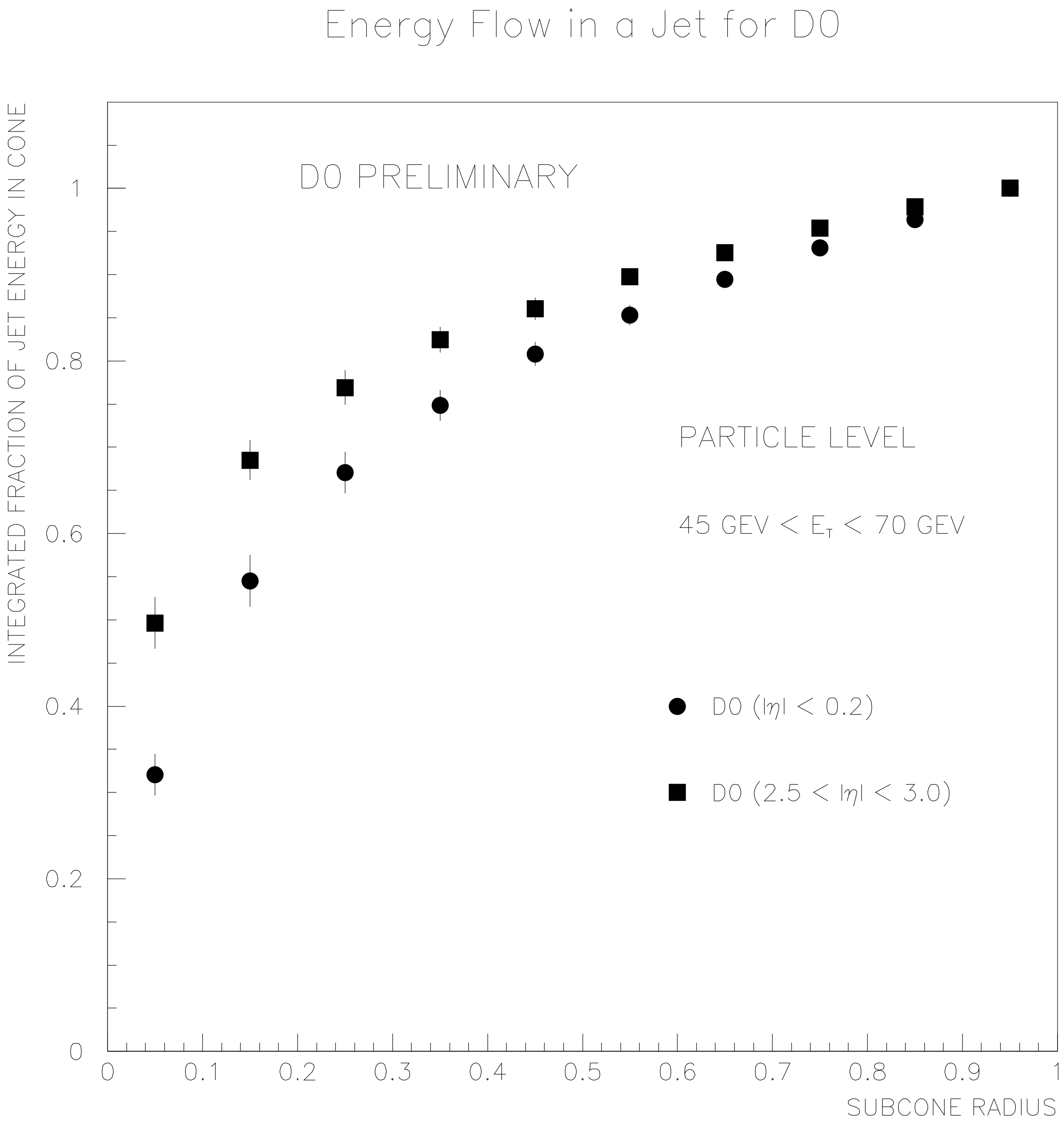

Figure 15: Forward jets vs central jets after the affects of the calorimeter have been removed for 45-70 GeV jets.

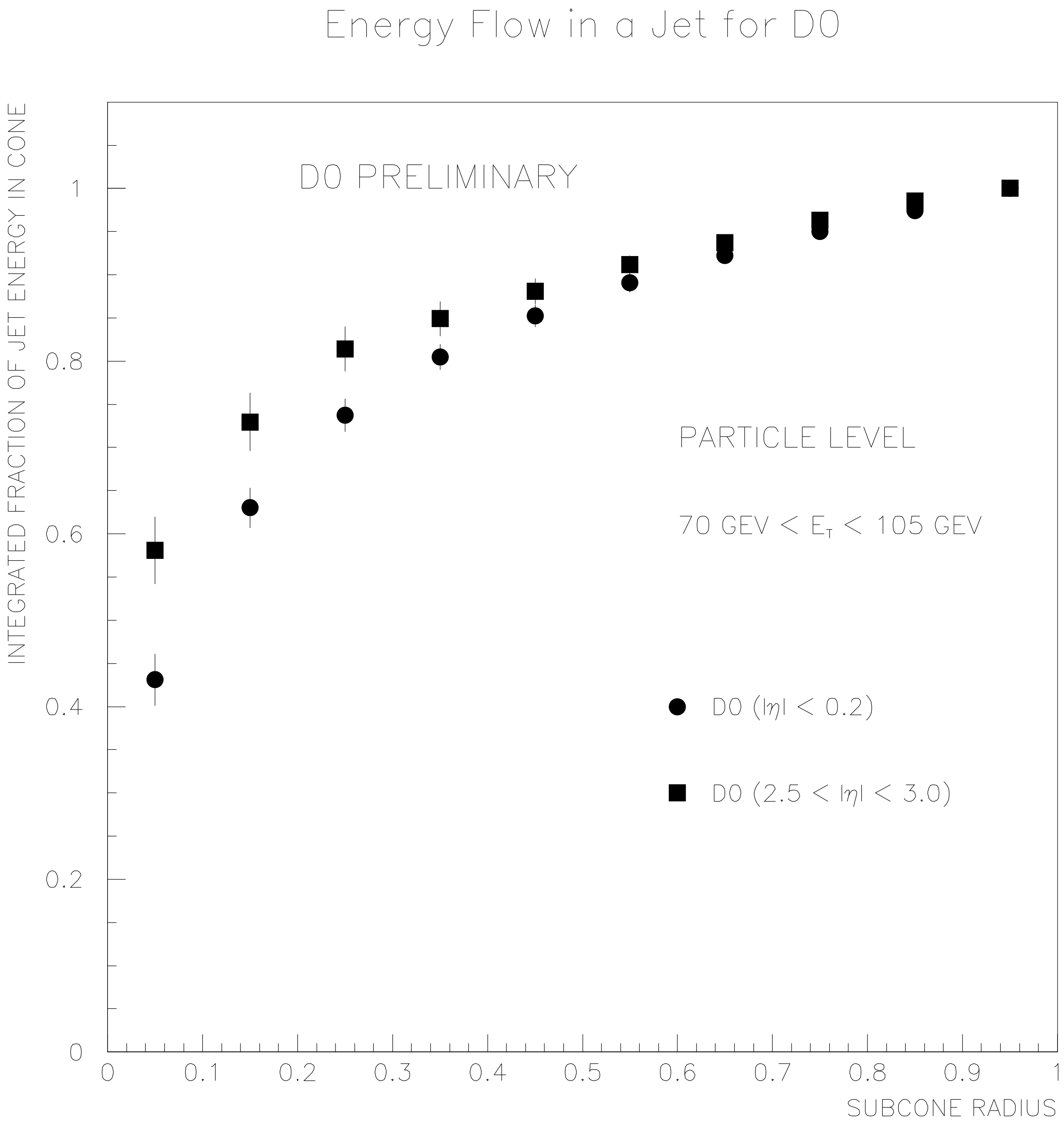

Figure 16: Forward jets vs central jets after the affects of the calorimeter have been removed for 70-105 GeV jets.

effects of changing struture functions. Figures 17 - 20 compare the collider data in the central region to theory for the three different renormalization scales. The corrections to remove calorimeter effects were made to the data. Although the data fall within the different curves, no one renormalization scale describes the data for all E_T. The effect of changing renormalization scale is quite large.

Figure 21 compares theory to collider data in the forward region. Again the data fall within the different curves, but no one renormalization scale describe the data.

6 Comments and Conclusions

Jets should narrow as the E_T of the jet increases since the transverse momentum of particles within the jet changes slowly with energy and the parallel momentum of particles within the jet changes approximately with energy. Forward jets are narrower then central jets at the same E_T. It is expected that there are more quark jets at higher η. This is because in order to get a di-jet event at high η, one parton must have a low momentum fraction and one parton must have a high fraction. Gluons very rarely have a high momentum fraction, so the gluon-gluon contribution at high η diminishes, giving an enhanced quark sample. Quark jets are expected to be narrower than gluon jets because gluons, carrying more color than quarks, emit gluons more readily than quarks. The more partons emitted, the wider the jet. Kinematic effects also occur when comparing central to forward jets so the difference is not totally due to differences between quark and gluon jets.

This measurement cannot be made at LO. The jet shape measurement is a first order measurement at NLO and large effects on the renormalization scale are expected. NLO theory qualitatively agrees with data. It correctly predicts the narrowing of jets as the E_T of the jets increase. It also correctly predicts the narrowing of jets as η increases. Quantitatively, NLO cannot describe the jet shape accurately. By changing the renormalization scale, it may be possible to correctly describe the jet shape at one particular E_T and η region. Either higher orders must be taken into account or the effects of fragmentation are not negligible and must be included when calculating jet shapes.

There are many further studies which can be made with jet shapes. It should be possible to measure the differences between quark and gluon jets. Knowing the shape of quark jets could reduce backgrounds for different analyses, including top to all jets and W to jets. A comparison to jets from e^+e^- experiments could determine if jets produced at a hadron collider are different from jets produced at an electron collider.

6.1 Appendix

A PBD package, EFLOW, was written and included in the CALOR_OFF framework along with the CAHITS, CAJETS and ZTRAKS packages. The data used were from the DØ Run 1A QCD micro DSTs (MDST). The JTCS

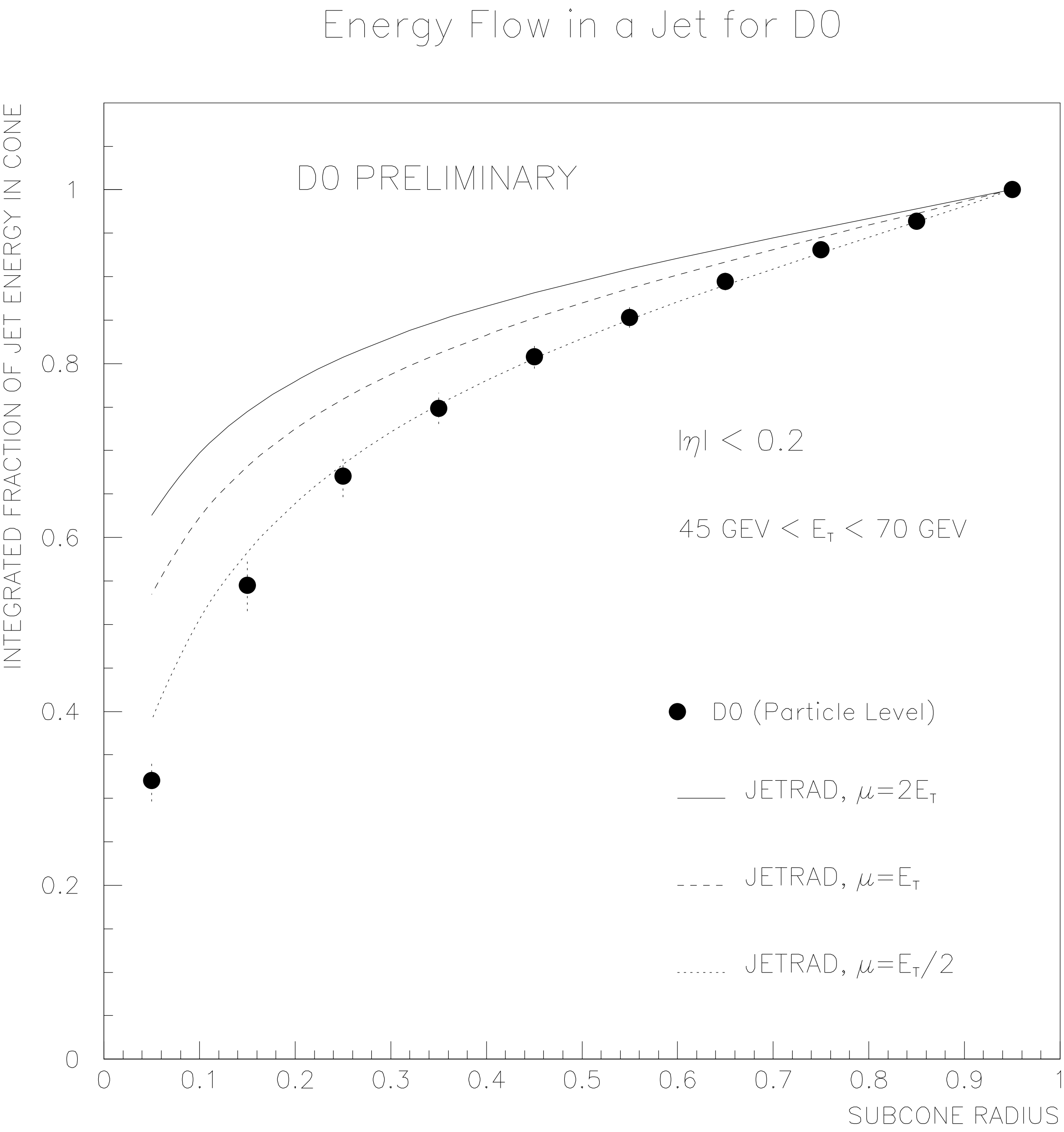

Figure 17: Comparing data to theory in the central region for 45-70 GeV jets.

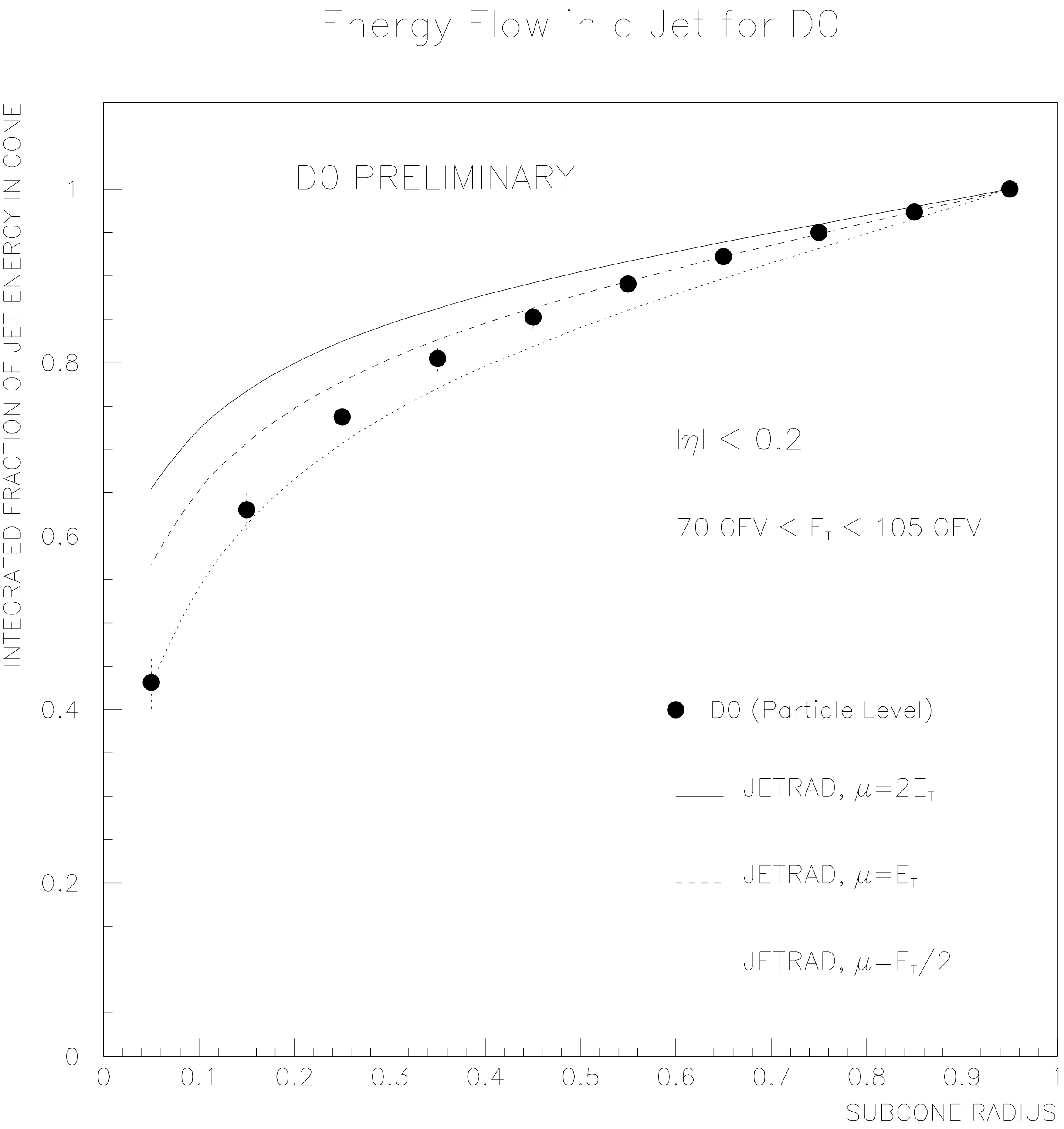

Figure 18: Comparing data to theory in the central region for 70-105 GeV jets.

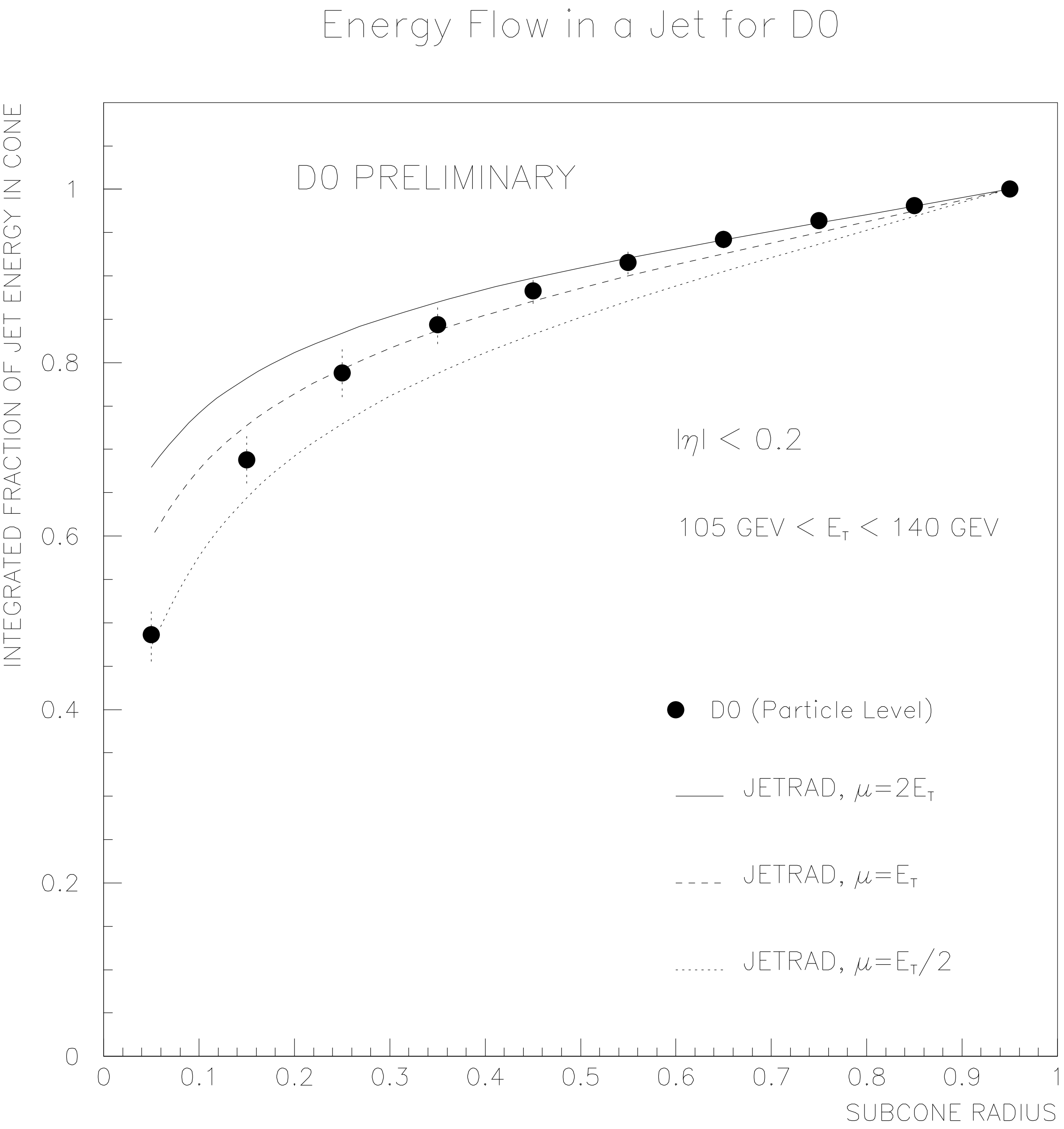

Figure 19: Comparing data to theory in the central region for 105-140 GeV jets.

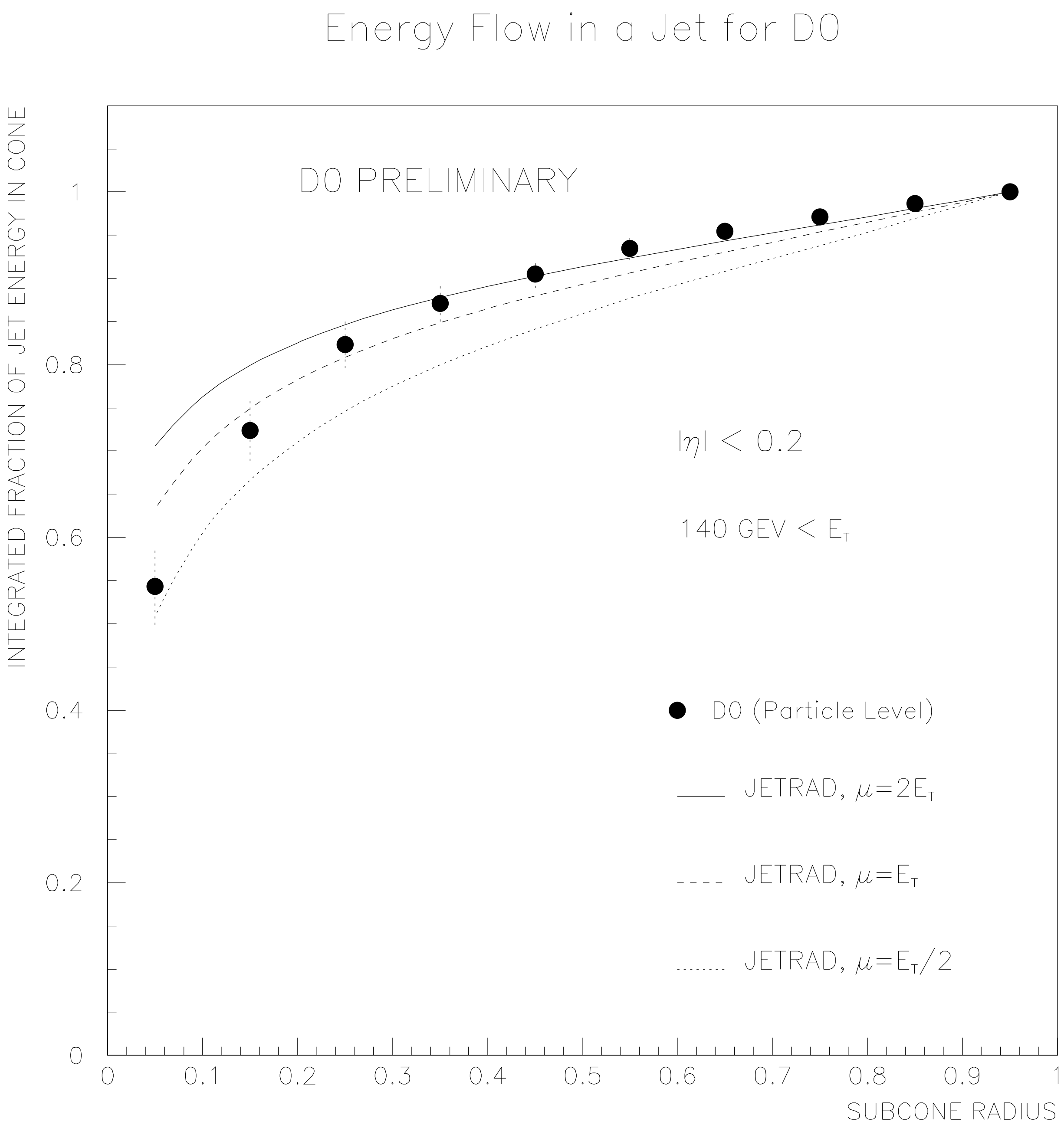

Figure 20: Comparing data to theory in the central region for 140- GeV jets.

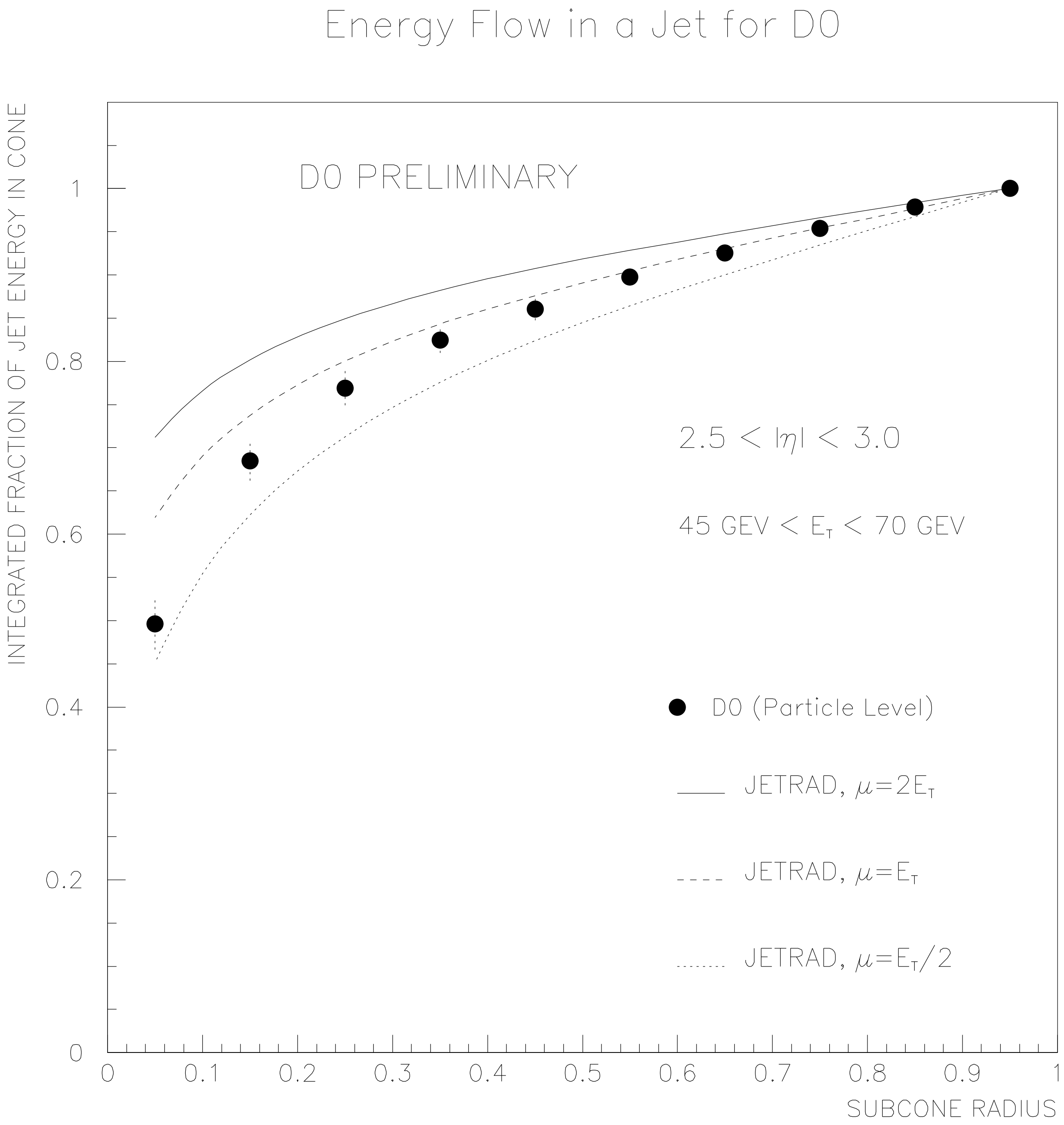

Figure 21: Comparing data to theory in the forward region for 45-70 GeV jets.

bank, which is created in the routine CAJETS_ADDON during reconstruction, contains the transverse energy as a function of distance from the jet axis for each jet in the event. The jet cone size is given in the CAJETS_RCP file. Since the jets in JTCS were not E_T-ordered as they are in the JETS bank, the JTCS bank was reordered. This was necessary for correlating jets in the JTCS bank to jets in the JETS bank.

References

[1] The Two-Jet Differential Cross Section at O(α_s^3) in Hadron Collisions. W.T. Giele *et al*, Fermilab-Pub-94/070-T

[2] Measurment of Jet Shapes in $p\bar{p}$ Collisions at $\sqrt{s}$=1.8 TeV. F. Abe *et al*, Phys Rev Lett, Vol 70, Number 6, 713 (1993)

[3] A study of differences between quark and gluon jets using vertex tagging of quark jets. OPAL Collaboration, CERN-PPE/93-02, (1993)

[4] *Toward a Standardization of Jet Definition*, S.D Ellis, J. Huth, N. Wainer, K. Meier, N. Hadley, S. Soper and M. Greco, Proceedings of *Research Directions For The Decade, Snowmass 1990*, Snowmass, July 1990, ed. E.L. Berger, p.134, (World Scientific, Singapore, 1992)

[5] V. Elvira *et al*, DØ internal note #1763

[6] B. Kehoe, DØ internal note #2052

[7] W.T. Giele,E.W.N. Glover,D.A. Kosower